World Academy of Science, Engineering and Technology
International Journal of Chemical and Molecular Engineering
Vol:9, No:2, 2015

Photocatalytic Degradation of Organic Pollutant Reacting with Tungstates: Role of Microstructure and Size Effect on Oxidation Kinetics

A. Taoufyq, B. Bakiz, A. Benlhachemi, L. Patout, D. V. Chokouadeua, F. Guinneton, G. Nolibe, A. Lyoussi, J-R. Gavarri

***Abstract*—**The aim of this study was to investigate the photocatalytic activity of polycrystalline phases of bismuth tungstate of formula Bi_2WO_6. Polycrystalline samples were elaborated using a coprecipitation technique followed by a calcination process at different temperatures (300, 400, 600 and 900°C). The obtained polycrystalline phases have been characterized by X-ray diffraction (XRD), scanning electron microscopy (SEM), and transmission electron microscopy (TEM). Crystal cell parameters and cell volume depend on elaboration temperature. High-resolution electron microscopy images and image simulations, associated with X-ray diffraction data, allowed confirming the lattices and space groups $Pca2_1$. The photocatalytic activity of the as-prepared samples was studied by irradiating aqueous solutions of Rhodamine B, associated with Bi_2WO_6 additives having variable crystallite sizes. The photocatalytic activity of such bismuth tungstates increased as the crystallite sizes decreased. The high specific area of the photocatalytic particles obtained at 300°C seems to condition the degradation kinetics of RhB.

***Keywords*—**Bismuth tungstate, crystallite sizes, electron microscopy, photocatalytic activity, X-ray diffraction.

I. Introduction

THE increased and uncontrolled use of pesticides in the agricultural sector threatens the stability of ecosystems and human health. Indeed, Pesticides can spread through volatilisation on the atmosphere upon application. Residues can contaminate soil and groundwater. Hence, we need urgent and effective solutions to address these residues by eliminating the active ingredient. Currently, the photocatalytic reactions occurring under solar illumination have attracted worldwide attentions due to a tremendous set of environmental problems. Taking the sunlight into account, it is indispensable to develop highly effective visible-light-driver photocatalysts. Semiconductor photocatalysis has become the focus of investigations due to its potential applications for solar energy conversion and environmental purification [1], [2]. To date, the semiconductor TiO_2 has undoubtedly proven to be one of the most excellent photocatalysts for the oxidative decomposition of many organic compounds [3], [4]. But, due to its wide band-gap of 3.2 eV, TiO_2 can only be excited by ultraviolet or near-ultraviolet radiation, which occupies only about 4% of the solar light spectrum [5], which limits his application into practice. Recently, the bismuth tungstate has been found to have excellent photocatalytic activity under visible-light irradiation when used to decompose water dyes and indoor pollutants [6]-[10]. In addition, the bismuth tungstate phase Bi_2WO_6 is a typical multifunctional material presenting several properties: luminescence under UV or X-ray excitation [11], piezoelectricity and ionic conduction [12]; recently we have studied the electrical conductivity and showed that this phase showed a major ion conduction at high temperature.

The general aim of this study is to contribute, firstly, to the study of the structure of this layered compound, and, secondly, to try establishing clear correlations between the microstructure, the crystallite sizes and photocatalytic activity of bismuth tungstate against Rhodamine B.

II. Experimental

A. Synthesis

The elaboration conditions were previously developed in our work of the electrical conductivity of this phase [11]. Samples of bismuth tungstate phase Bi_2WO_6 were produced using the co precipitation method. We just recall here the main steps of syntheses. The preliminary precursors were bismuth nitrate and ammonium tungstate in aqueous solutions. The pentahydrate Bismuth (III) nitrate $Bi(NO_3)_3$, $5H_2O$ was dissolved in a volume of diluted HNO_3 (10% v/v) at 25°C. This nitrate solution was slowly added to 0.1 L of an aqueous solution of $(NH_4)_{10}(W_{12}O_{41})$, $6H_2O$ under vigorous stirring. Ammonium hydroxide (NH_4OH) was added to the solution in order to adjust the pH (pH = 5). The mixture was stirred and kept in a water bath around 70 to 80°C, in order to obtain a slow evaporation of water until the formation of a white solid, which was used as final precursor. Finally, this precursor powder was thermally treated at 300, 400, 600 and 900°C, in air for 4 hours.

A. Benlhachemi and B. Bakiz are with the IBN ZOHR University, Faculty of sciences, Environment and Materials Laboratory, Agadir, Morocco (phone: + 212661532238, e-mail: a.benlhachemi@gmail.com, bakiz.lahcen@hotmail.fr).

A. Taoufyq and J-R. Gavarri are with the University of Toulon, IM2NP, UMR CNRS 7334, La Garde, France (e-mail: taoufyq@univ-tln.fr, gavarri.jr@univ-tln.fr).

L. Patout, D. V. Chokouadeua, and F. Guinneton are with the University of Toulon, IM2NP, UMR CNRS 7334, La Garde, France (e-mail: patout@univ-tln.fr, vyoumssy@gmail.com, guinneton@univ-tln.fr).

G. Nolibe is with the Cesigma society, signals & systems, La Garde, France (e-mail: gno@cesigma.com).

A. Lyoussi is with the CEA of Cadarache, Instrumentation Sensors and Dosimetry Laboratory, France (e-mail: abdallah.lyoussi@cea.fr)

B. Characterization Techniques

X-ray Diffraction

The samples were analyzed by X-ray diffraction (XRD), using an EMPYREAN Panalytical diffractometer, equipped with a copper X-ray source (wavelength $\lambda = 1.54.10^{-10}$ m, tension V = 45 kV, intensity I = 35 mA), a Ni filter eliminating the Kβ radiation and a rotating sample holder. The diffractometer was equipped with a Pixcel-1D-Detector. The XRD analysis was carried out using the classical θ–2θ configuration, in continuous mode, with a step size of 0.00164, a scan speed of 0.002°/s. The diffraction profiles were analyzed using the Winplotter program [13]. The lattice parameters were refined using the PARAM program [14] based on least squares method. The crystal structure of the sample treated at 900°C has been refined using Rietveld method [13]. The average crystallite's size of the prepared powders was evaluated from the half-widths of diffraction peaks using the Scherrer formula [15]-[17].

$$D = \frac{K.\lambda}{\beta.cos(\theta)}$$

where λ is the wavelength of X-ray ($\lambda_{CuK\alpha 1} = 1.54 \times 10^{-10}$m); K is a Scherrer constant (K = 0.9 in this case); θ is the diffraction angle associated with a Bragg peak; $\Delta 2\theta = (\Delta 2\theta_m^2 - \Delta 2\theta_s^2)^{1/2}$ is the corrected full width at half maximum (FWHM), $\Delta 2\theta_m$ being the total FWHM of the Bragg peak, $\Delta 2\theta_s$ being that of a standard crystallized sample of Bi_2WO_6.

Microstructural Techniques

Scanning and transmission electron microscopy (SEM, TEM) analyses were used to observe the nanoparticle morphology. Preliminary images were obtained with a SUPRA 40 VP COLONNE GEMINI ZEISS SEM using a maximum voltage of 20 kV. HREM images, Electron Diffraction (ED) patterns and EDS analyses were obtained with a LaB_6 FEI Tecnai transmission electron microscope (TEM) operated at 200 kV. The super-twin objective lens has a 0.25 nm point-to-point resolution. Crystallographic image processing (CIP) was applied to experimental HREM maps, with the CRISP software [18]. Theoretical HREM images and ED patterns were simulated with the JEMS software [19].

Photocatalytic Activity Tests

Degradation process was studied as a function of irradiation time and the experimental procedure was decomposed in two main steps: (a) irradiation of standard aqueous solutions of RhB without photocatalytic BWO phase; (b) irradiation of solutions of RhB in presence of BWO (and doped BWO) powders in various concentrations. The light source was a Xenon lamp working at 190 W. To determine the degradation of RhB, a UV-Visible-1800 SHIMADZU spectrometer was used to analyze the evolution of absorption bands as a function of irradiation time. At given intervals, a small amount of suspension was taken out and filtered to remove the solid particles, and the filtrates were collected for analysis.

III. Results and Discussion

A. Structural Study

Fig. 1 shows the obtained diffractogrammes of pure bismuth tungstate calcined at different temperatures.

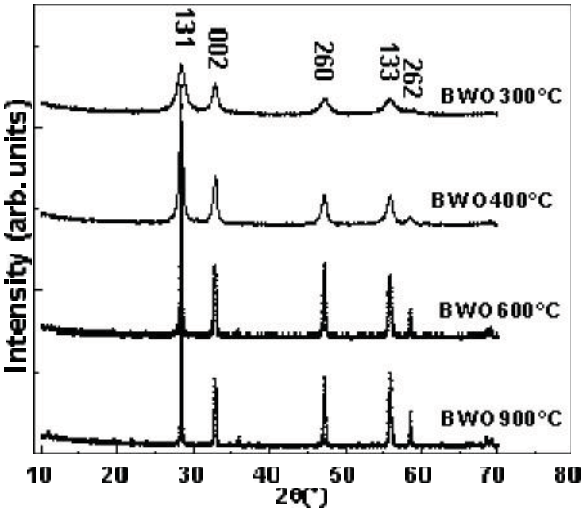

Fig. 1 X-ray diffraction patterns of pure bismuth tungstate obtained at different calcination temperature

X-ray diffraction patterns revealed that all peaks are indexed in Bi_2WO_6 aurivillius structure (JCPDS-79-2381). The XRD peaks became gradually sharper with increasing temperature and the average crystallite size increased from 14 to136 nm for temperatures of 300 and 900 °C respectively, indicating that the crystallinity of Bi_2WO_6 is accelerated by calcination process. In Table I, the lattice parameters, the crystallite size D calculated by Scherrer formula and specific surfaces were reported. The specific surfaces are calculated from an approximation of cubic grains: As = S / μV where S and V successively designate the surface and volume of a cubic medium grain, μ is the theoretical density.

TABLE I
Lattice Parameters, Crystallite Size (D) and Specific Surfaces of Bi_2WO_6 Obtained at Different Calcination Temperature

	BWO 300°C	BWO 400°C	BWO 600°C	BWO 900°C
a (Å)	5.39(3)	5.41(3)	5.433(4)	5.434(3)
b (Å)	16.27(6)	16.34(9)	16.41(1)	16.424(8)
c (Å)	5.41(6)	5.46(2)	5.457(5)	5.456(4)
V(Å^3)	475 (3)	482(4)	486.7(7)	487.0(5)
D (nm)	14 (3)	17 (4)	35 (6)	136 (25)
As (m^2/g)	45 (9)	37 (7)	18 (4)	4.6 (0.8)

Fig. 2 illustrates the relationship between the calcination temperature and the average crystal size of Bi_2WO_6 compounds. It can be seen that the crystallite size increases with increasing calcination temperature and becomes especially more large in the range of 600-900 °C.

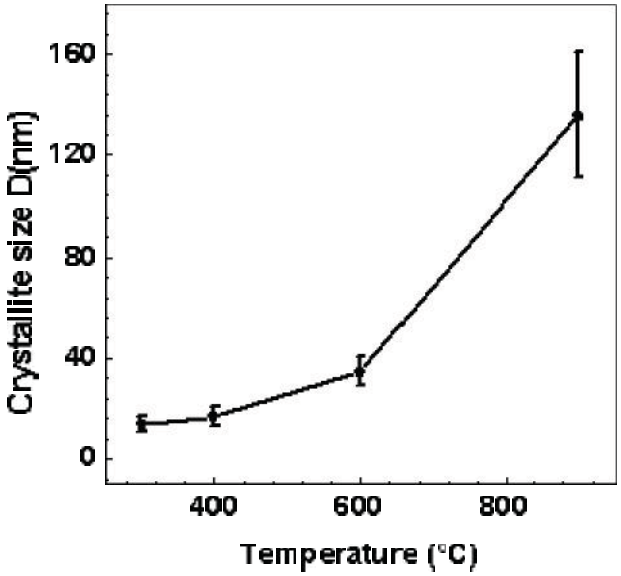

Fig. 2 Effect of calcination temperature on the crystallite sizes of Bi_2WO_6 phases

The crystal structure of the sample treated at 900°C has been refined using Rietveld method [13]. The refinement results were obtained using the space group $Pca2_1$. The observed and calculated profiles of the sample treated at 900°C are shown in Fig. 3. The difference curve shows a good agreement between the observed and calculated patterns.

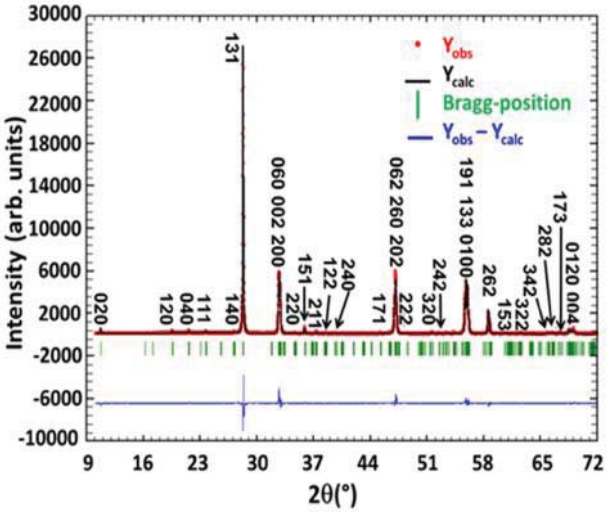

Fig. 3 Calculated and observed diffraction profiles from Rietveld analysis for the Bi2WO6 phase (space group Pca21), thermally treated at 900°C

B. Scanning Electron Microscopy

The scanning electron experiments reported on Figs. 4 (a)-(d) show that the structural evolutions observed from XRD experiments are associated with strong modifications in morphology in sample heated at 300°C and 900°C. The EDX local microanalysis is congruent with the chemical composition of Bi_2WO_6 with presence of gold due to the metallization for SEM analysis. The ratio Bi/W is constant.

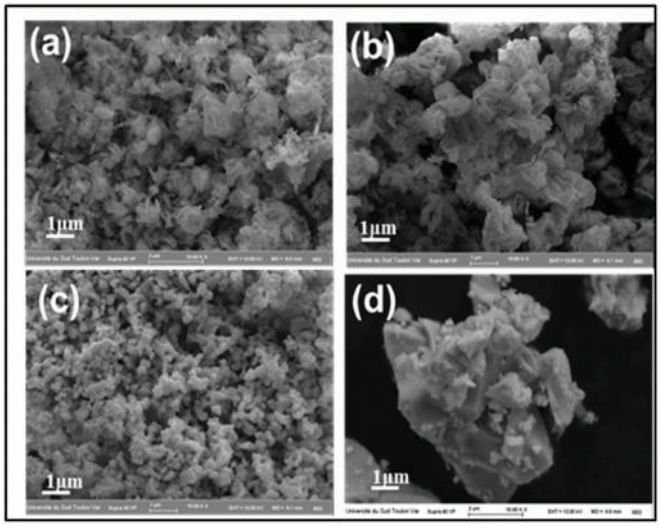

Fig. 4 Scanning electron microscopy analysis of Bi2WO6 treated at (a), 300°C (b), 400°C (c) 600°C and (d) 900°C

C. TEM and HREM Analysis

The main objective of these experiments was to confirm (or not) the space group and the disordered nature of this phase at the local scale. Selected area electron diffraction (SAED) patterns were recorded in the main orientations corresponding to the [100], [010] and [001] zone axes of the orthorombic system (Figs. 5 (a)-(c). The simulated patterns (Figs. 5 (d)-(f), calculated using the space group $Pca2_1$ and the lattice parameters show positions of simulated reflections in agreement with the experimental results.

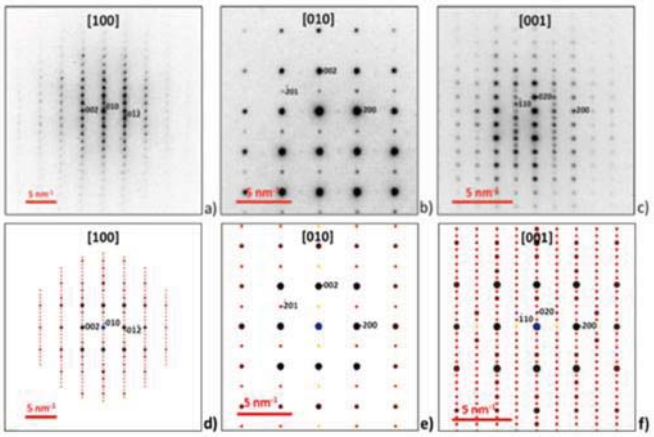

Fig. 5 (a)-(c) Experimental Electron Diffraction patterns of highest symmetry of the orthorhombic structure and (d)-(f) simulated patterns by the JEMS software

Experimental HREM maps were recorded in [100] and [001] zone axes and processed with the software CRISP. Figs. 6 (a)-(d) represent the experimental HREM map and corresponding processed direct image in [100] and [001] zone axis respectively. The structures projections created by Carine software are also presented. We clearly observe the layered structure with the successive sandwiches $\{Bi_2O_2^{2+}\}$ and $\{WO_4^{2-}\}$.

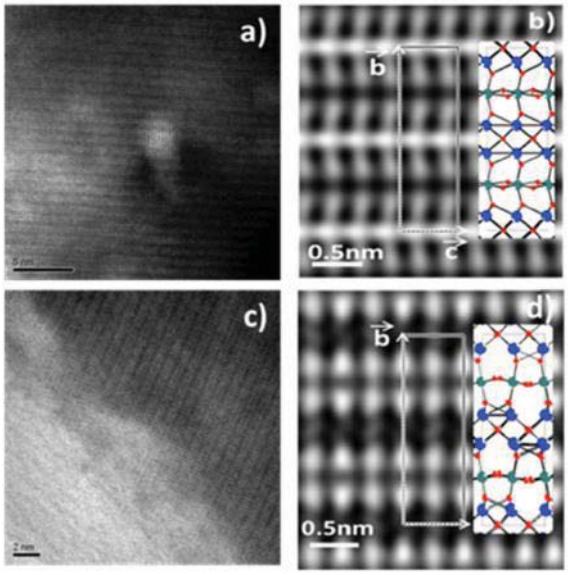

Fig. 6 Experimental HREM map and corresponding processed direct image in, (a), (b) [100] and (c), (d) [001], zone axis. The structures projections created by Carine software

D. Photocatalysis of the RhB

Degradation of Rhodamine B in the presence or absence of BWO photocatalyst was determined by following the evolution, over time, of the characteristic absorption band of the RhB, whose maximum is located at the wavelength λ_{max} = 554 nm.

Fig. 7 summarizes the results for an RhB solution without catalyst (Fig. 7 (a)) and with BWO catalyst treated at 300 °C (Fig. 7 (b)). No degradation is observed for a solution without catalyst.

Fig. 8 (a) shows the variations of wavelengths (λ_{max}) versus time for the four samples BWO variable size (treated between 300°C and 900°C). Degradation for the solution with the catalyst treated at 300°C (crystallite size D=14 nm, and therefore high specific surface) is characterized by a wavelength shift of 554-496 nm coupled with a variation in intensity and shape of the strip. Degradation for the solution with BWO catalyst treated at 400°C is similar to the previous one but less pronounced (due to the size D of 17 nm). Degradation associated BWO catalyst treated at 600 ° C (size D of 35 nm) is less pronounced, with a lower variation of λmax. Finally, the degradation associated with BWO catalyst treated at 900°C (D=136 nm) is low.

High variation of λ_{max} is observed with a decrease even more rapidly even the size of the diffracting areas is lower. Thus, there is a progressive modification of the molecular structure of the RhB with formation of intermediate molecular previously described in the literature [20]. For BWO300 and BWO400 catalysts, there will be stabilization of an intermediate characterized by λ_{max}=496 nm. For BWO600 and BWO900 catalysts, the intermediate species (not stabilized) is linked to λ_{max} of 535.5 nm.

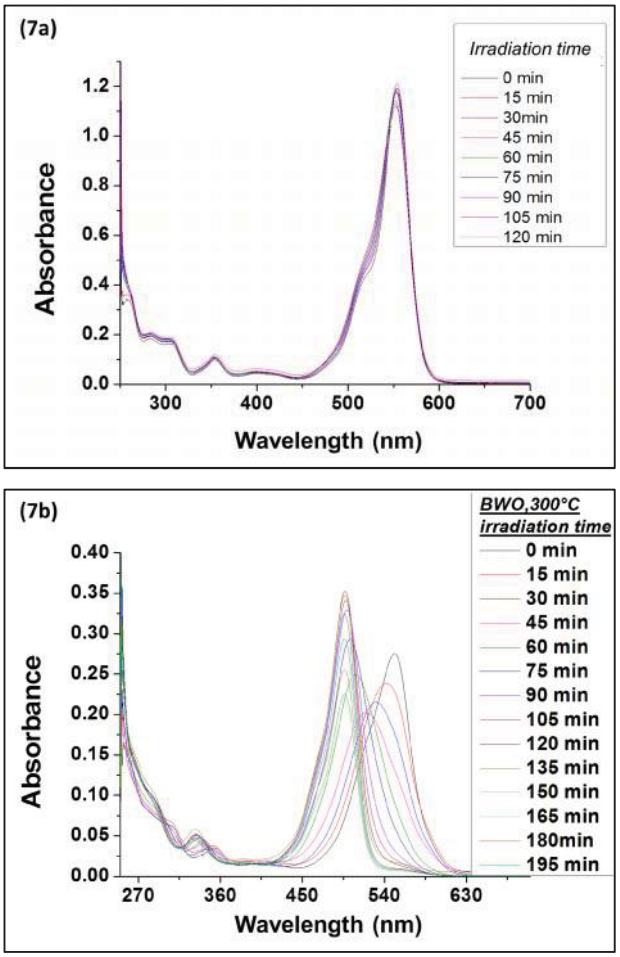

Fig. 7 Evolution of the absorption bands of RhB solutions under irradiation as a function of time, (a) with the presence or (b) not of Bi_2WO_6 catalysts treated at 300°C

Fig. 8 (b) shows the variation of the maximum absorbance A_{max} over time for various samples. For BWO catalysts, there is a drop in absorbance A_{max} correlated with decreased λ_{max} quantitatively reflecting the gradual transformation of the original molecule of RhB. These results mean that BWO300 degrade more rapidly Rhodamine solution than the other samples and generates more molecular intermediates.

The very small photocatalytic activity of the sample BWO900 can be explained by the poor dispersion of the sample in the Rhodamine solution [21]. Indeed, during the irradiation a fraction of the powder is accumulated in the bottom of the beaker due to its high density which influences the kinetics of degradation under irradiation.

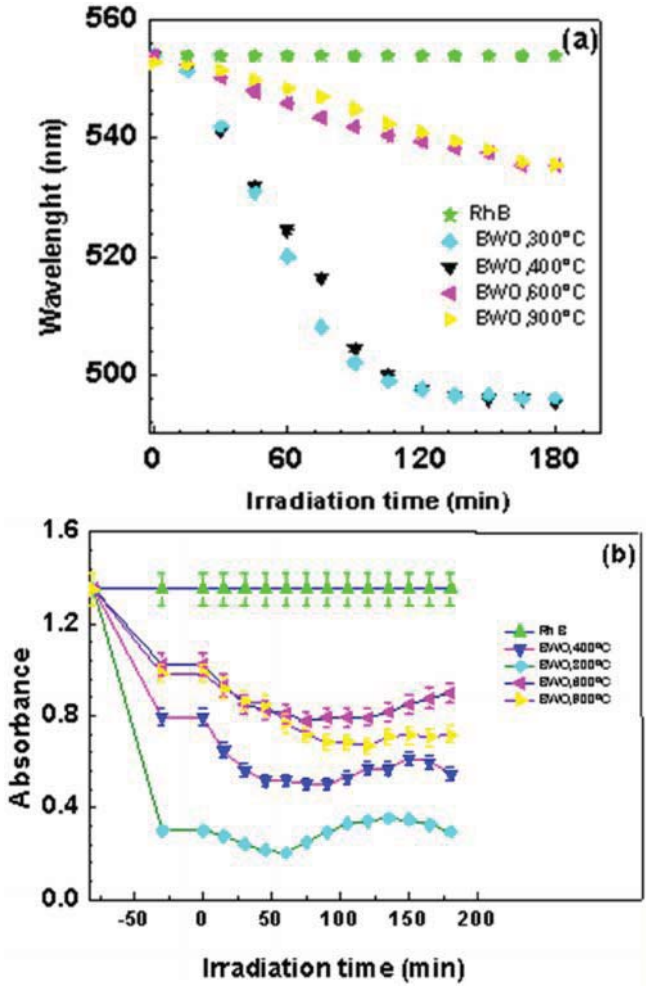

Fig. 8 (a) Variation of wavelength of a solution of RhB with Bi_2WO_6 catalysts under irradiation and (b) Evolution of the absorbance of the system, as a function of time

IV. Conclusion

By modifying the calcination temperature of precursors, we have established a good correlation between crystallite sizes and catalytic efficiency. The most remarkable observation is the continuing evolution of the degradation of RhB over time. Using the results of other authors performed differently, we show that the trend observed for the BWO photocatalyst obtained at 300°C can be interpreted by the gradual decomposition of RhB in intermediate molecules.

Acknowledgments

This work was financially supported by the Regional Council of Provence-Alpes - Côte d'Azur, the European Funds for Regional Development, the General Council of Var and by Toulon Provence Mediterranean, in the general framework of NANOGAMMA project (Grant number : 2010-16028/42169 ; collaboration between IM2NP, CEA of Cadarache, CESIGMA and IBS Societies) and international ARCUS-CERES project. This study was also developed in the general framework of CNRS-CNRST project (2014).

References

[1] A. Fujishima, K. Honda, Nature 238 (1972) 37-38.
[2] J.M. Herrmann, Catal. Today 53 (1999) 115-129.
[3] M.A. Fox, M.T. Dulay, Chem. Rev. 93 (1993) 341-357.
[4] M. Saquib, M. Muneer, Dyes and Pigments 56 (2003) 37-49.
[5] X.B. Chen, S.S. Mao, Chem. Rev. 107 (2007) 2891–2959
[6] J.W. Tang, Z.G. Zou, J.H. Ye, Catal. Lett. 92 (2004) 53-56.
[7] J.G. Yu, J.F. Xiong, B. Cheng, Y. Yu, J.B. Wang, J. Solid State Chem.178 (2005) 1968-1972.
[8] H.B. Fu, C.S. Pan, W.Q. Yao, Y.F. Zhu, J. Phys. Chem. B 109 (2005) 22432-22439.
[9] Z. He, C. Sun, S. Yang, Y. Ding, H. He, Z. Wang, hazard. Mater.162 (2009) 1477-1486.
[10] S. Murcia López, M.C. Hidalgo, J.A. Navío, G. Colón, hazard. Mater. 185 (2011) 1425-1434.
[11] S. Obregon Alfaro, A. Martinez-De La Cruz, Appl. Catal., A 383 (2010) 128-133.
[12] A. Taoufyq , H. Ait Ahsaine , L. Patout , A. Benlhachemi, M. Ezahri, F. Guinneton, A. Lyoussi, G. Nolibe, J-R. Gavarri, J. Solid State Chem. 203 (2013) 8-18.
[13] T. Roisnel, J. Rodrı´guez-Carvajal, in: R. Delhez, E. J. Mittenmeijer (Barcelona, Spain) (Eds.), Proceedings of the Seventh European Powder Diffraction Conference (2000) 118–123.
[14] J.F Berar, Ecole Centrale de Paris, 92295 Châtenay-Malabry Private Communication (1989).
[15] Cullity B.D, edition Addison-Wesley Publishing Co (1956) 98-99.
[16] Pullar, R.C., Taylor M.D., Bhattacharya, A.K., J. Eur. Ceram. Soc. 18 (1988) 1759-1764.
[17] Azàroff L.V., McGraw-Hill, New-York (1968) 331-568.
[18] S. Hovmöller, Ultramicroscopy. 41 (1992) 121-135.
[19] P. Stadelmann, Ultramicroscopy. 21 (1987) 131-146
[20] P. Dumrongrojthanath, T. Thongtem, A. Phuruangrat, S. Thongtem, Superlattices and Microstruc. 54 (2013) 71–77.
[21] H. Fu, L. Zhang, W. Yao, Y. Zhu, Appl. Catal., B. 66 (2006) 100-110.